Ancient Micrometeorites Suggestive of an Oxygen-Rich Archaean Upper Atmosphere

Andrew G. Tomkins[1], Lara Bowlt[1], Matthew Genge[2,3], Siobhan A. Wilson[1], Helen E.A. Brand[4], Jeremy L. Wykes[1,4,5]

1. School of Earth, Atmosphere & Environment, Monash University, Melbourne, Victoria 3800, Australia.
2. Impact and Astromaterials Research Centre, Department of Earth Science and Engineering, Imperial College London, Exhibition Road, London SW7 2AZ, UK.
3. Department of Mineralogy, The Natural History Museum, Cromwell Road, London SW7 2BT, UK.
4. Australian Synchrotron, 800 Blackburn Road, Clayton, Victoria 3168, Australia.
5. Department of Earth and Planetary Sciences, Macquarie University, North Ryde, New South Wales 2113, Australia.

*Corresponding Author Details:

Email: andy.tomkins@monash.edu

Phone: +61 3 9905 1643

Fax: +61 3 9905 4903

It is widely accepted that Earth's early atmosphere contained less than 0.001% of the present-day atmospheric oxygen (O_2) level, until the 'Great Oxidation Event' resulted in a major jump in O_2 concentration ~2.4 billion years ago[1]. There are multiple strong lines of evidence for low O_2 concentrations on early Earth, but all previous observations relate to the composition of the lower atmosphere[2]; to date no method has been developed to sample the Archaean upper atmosphere. Here, we extract fossil micrometeorites from limestone sedimentary rock that had accumulated slowly 2.7 billion years ago before being preserved in Australia's Pilbara region. We propose that these micrometeorites formed when sand-sized particles entered Earth's atmosphere and melted at altitudes of ~75–90 km (given similar atmospheric density to today[3]). Our observations reveal that the FeNi metal in the resulting cosmic spherules was oxidised whilst molten and quench crystallised to form spheres of interlocking dendritic crystals of primarily magnetite (Fe_3O_4), with wüstite (FeO) + metal preserved in a few particles. Our model of atmospheric micrometeorite oxidation suggests that Archaean upper atmosphere oxygen concentrations may have been close to those of the modern Earth, and that the oxygen to carbon monoxide ratio was sufficiently high to prevent noticeable inhibition of oxidation by carbon monoxide. The anomalous $\Delta^{33}S$ signature of pyrite (FeS_2) in sea floor sediments from this period, requiring an anoxic surface environment[4], implies that there was minimal mixing between the upper and lower atmosphere during the Archaean.

The low concentration of O_2 in Earth's lower atmosphere during the Archaean period (3.9–2.5 Ga) has been demonstrated through (1) preservation of detrital pyrite and uraninite in ancient sediments derived from weathering of rocks on land (these weather

rapidly in the presence of oxygen[5]), (2) a lack of oxidised iron in paleosols[6], and most definitively, (3) the strong mass-independent fractionation (MIF) of sulfur isotopes recorded in seafloor pyrite[4]. In addition, significant volumes of banded iron formations in late Archaean sedimentary rock sequences require that high concentrations of dissolved Fe^{2+} existed in the Archaean oceans, which buffered atmospheric and oceanic O_2 to very low concentrations[7]. After the evolution of photosynthesising bacteria (possibly at ~2.7 Ga[8,9]), this balance was maintained while there was sufficient dissolved Fe^{2+} in seawater, which was likely facilitated by particularly active volcanism in the period 2.7–2.4 Ga[7]. The highly variable $\Delta^{33}S$ signature of pyrite (FeS_2) in carbonaceous shales from this period is evidence that volcanically released SO_2 was UV dissociated in the atmosphere and then never re-oxidised; this requires that the O_2 concentration was <0.001% of the present atmospheric level[4]. The Great Oxidation Event is thought to have occurred when the rate of O_2 production outstripped the rate of removal via iron oxide sedimentation[1], as a consequence of increased bacterial colonisation and decreased volcanic activity[7,10]. After 2.4 Ga the $\Delta^{33}S$ of pyrite is invariant, indicating that atmospheric O_2 had significantly increased[11].

Sulfur has been injected continuously into Earth's atmosphere by volcanic eruptions over geologic time. In the case of the largest ultraplinian eruptions, ejection columns can reach the upper stratosphere, to heights of 50 km[12]. Today, volcanic material from a single eruption may remain in the stratosphere for years because there is little mixing within this layer[13]. On the other hand, micrometeorites entering the modern atmosphere experience their peak temperature at 75–90 km[14] as they are decelerated from velocities exceeding 12 km s^{-1} between 80 and 150 km altitude[15]. For those micrometeorites that were sufficiently heated to melt completely (70–90% of modern micrometeorites >100 μm are completely melted, whereas ~22% of those 25–50 μm in size are fully or partially

melted[16]), their high surface area results in quench crystallisation as they cool at the end of deceleration. Because small micrometeorites are melted and quench crystallised within two seconds, modern micrometeorites only strongly chemically interact with higher levels of the atmosphere. Therefore, we suggest that fossil micrometeorites trapped in sedimentary rocks represent a previously untapped, long-term record of the chemical composition of Earth's upper atmosphere.

To obtain the oldest fossil micrometeorites yet found (the previous oldest fell 1.8 b.y. ago[17]), we sampled limestone layers from the Meentheena Member from the Pilbara region of northwest Australia. The 30–50 m thick Meentheena Member is part of the Tumbiana Formation in the Mount Bruce Supergroup of the Hamersley Basin[18]; its age is 2721 ± 4 Ma[19]. We chose this unit because, (1) it is barely affected by deformation and metamorphism, (2) its sediments were deposited slowly (deposition rate of ~45 m/m.y.[20]), thereby allowing greater accumulation of micrometeorites, and (3) limestone is easily dissolved with acid, allowing rapid extraction of micrometeorites from large samples. We preferentially selected samples from surface outcrops with fine horizontal laminations (from S21° 17' 43.8", E120° 27' 28.7"; Extended Data Fig. 1) because these imply a slow deposition rate in a calm, deeper-water setting.

Sixty micrometeorites, 8.6–50 μm in diameter, were separated from three limestone samples and examined by microanalytical techniques (see Methods). All extracted micrometeorites are cosmic spherules — meteoritic material that was fully melted during atmospheric entry. Fifty-nine of these are I-type (iron) cosmic spherules (i.e., they contain no silicate material, only FeNi metal and/or Fe oxide phases) and one is a 'glassy type' (i.e., devitrified silicate glass). I-type cosmic spherules represent meteoritic FeNi metal that melted and reacted with the atmosphere during deceleration, via oxidation of Fe to form wüstite and magnetite[16].

Figure 1 shows a representative selection of the recovered spherules; for comparison, examples of modern I-type spherules and weathered micrometeorites are shown in Extended Data Figure 2. The exterior of all I-type spherules consists of interlocking dendritic crystals of magnetite ($Fe^{2+}Fe^{3+}{}_2O_4$) and occasionally, less oxidised wüstite (FeO). Some spherules have limestone still attached, indicating that they cannot possibly represent modern contamination. The interiors of sectioned I-type spherules vary from being magnetite-only (9 of 11 micrometeorites) to wüstite with FeNi metal (2 of 11 micrometeorites; Fig. 1, Extended Data Table 1, Extended Data Fig. 3), identified via Wavelength Dispersive X-ray Spectroscopy (WDS) and Raman spectroscopy. Synchrotron Powder X-ray Diffraction on two additional micrometeorites found only magnetite throughout the entire volume of both micrometeorites (Extended Data Fig. 4).

Evidence that these are micrometeorites that were oxidised in the atmosphere, rather than products of diagenesis, metamorphism or later weathering includes: (1) the spheres of FeNi metal encased in wüstite (Fig. 1) confirm an extraterrestrial origin (FeNi metal does not form, and wüstite is rare, in sedimentary environments on Earth) and indicate quenching of a partially oxidised metallic liquid; (2) the spherical morphology and high surface area of the interlocking magnetite crystals indicate rapid crystallisation from a high surface tension liquid. These are typical of modern micrometeorites recovered from Antarctic ice[16] and the deep ocean[21], and inconsistent with oxidation of iron metal encased in sediment[22], where there is no mechanism to promote retention of the spherical shape (e.g., Extended Data Fig. 2e); (3) oxidation of metal during modern weathering produces hematite, ferrihydrite and goethite, and results in significant volume expansion that would destroy the delicate sub-micrometer surface textures shown in Figure 1.

Given their oxidised mineralogy, we designed a mathematical model to examine micrometeorite oxidation during atmospheric entry (see Methods). Molecules in the

Archaean upper atmosphere capable of causing oxidation of Fe metal include O_2 and CO_2 (Extended Data Fig. 5), whereas CO is the only moderately abundant species capable of causing reduction; other species were likely present at concentrations too low to be relevant[23]. Given that nearly all of the I-type cosmic spherules from the Meentheena Limestone contain dominant proportions of magnetite and/or wüstite relative to metal, the oxidising molecules must have dominated Earth's upper atmosphere 2.72 billion years ago. Equilibrium-based calculations imply that small micrometeorites cannot be oxidised to liquid magnetite by a CO_2-dominated atmosphere, and that some O_2 is required (Extended Data Fig. 5). But determining the relative concentrations of O_2 and CO_2 is challenging to model, because the short duration of atmospheric heating means that equilibrium is never reached. Nonetheless, experiments on high temperature iron oxidation in mixed gases show that oxidation in the presence of O_2 is rapid and readily forms magnetite + wüstite, whereas oxidation driven by CO_2 alone is slow and produces only wüstite (Extended Data Fig. 6)[24,25]. The predominance of magnetite in the Archaean micrometeorites thus implies that O_2 was an important oxidising species. Furthermore, experiments indicate that when oxygen is present, addition of CO_2 has little effect on brief oxidation events[24]. Our modelling therefore investigates how much oxygen would need to be present to generate the observed micrometeorite mineralogy.

Modelling of entry heating and oxidation of iron micrometeoroids is complicated by competition between Fe oxidation and evaporative removal of the iron-oxide exterior; evaporation is greater for larger particles, faster entry velocities and steeper entry angles (Extended Data Fig. 7). Nonetheless, due to the high temperatures, molten state and high surface area, reaction between metal and the atmosphere is rapid. Consequently, iron oxide-free metal spherules have not been found amongst thousands of modern

micrometeorites[26]. There are, however, modern examples of incomplete equilibration where a thick magnetite-wüstite shell surrounds a metal bead[16].

Figure 2 shows the results of atmospheric oxidation modelling for I-type spherules and demonstrates that significant survival of metal occurs when atmospheric oxygen abundance is lower than 0.2 times the present atmospheric level (PAL), particularly in the case of smaller spherules. In contrast, oxide- and particularly magnetite-dominated spherules are most abundant at atmospheric O_2 concentrations similar to the Earth's current atmosphere. The absence of metal in the majority of the sectioned Archaean spherules, coupled with their small size, therefore indicates that they formed by heating in an atmosphere with dramatically higher proportion of oxygen than the estimated surface concentration of oxygen at this time ($\leq 1 \times 10^{-5}$ PAL[4]). Assuming that current models of the Archaean lower atmosphere are accurate, our results imply strong decoupling of the lower and upper atmosphere at this time.

In today's atmosphere there is rapid, vigorous mixing below the tropopause (8-18 km), little vertical mixing within the stratosphere (vertical diffusivity is ~0.1 m^2/s; Ref. 27) below the stratopause (50-55 km), and moderate vertical mixing within the mesosphere up to the mesopause (85 km), above which there is minimal mixing again[13]. The extent of vertical atmospheric mixing is controlled by the thermal properties of the gases; because hotter air is less dense than colder air, mixing is inhibited where air temperature increases with altitude, as in the stratosphere where more UV is absorbed and converted to heat by ozone at higher altitudes (Fig. 3). Importantly, although mixing occurs within the mesosphere, there is minimal chemical communication between the altitude of maximum I-type micrometeorite heating (75–90 km) and that of volcanic flux (in the troposphere and stratosphere, 0–50 km)[13], largely due to the inverted temperature profile of the stratosphere. Our observations suggest that a similar atmospheric structure

with inhibited vertical mixing existed at 2.72 Ga. Kasting[23] suggested that biosphere–atmosphere interactions may have moderated the CH_4:CO_2 ratio to stabilise an Archean atmosphere with an optically thin organic haze; we suggest that in such an environment, methane would absorb heat and create an inverted temperature profile (e.g., Ref. 28) thereby suppressing mixing between the oxygen-poor lower and oxygen-rich upper atmosphere.

Some chemical models of the Archean atmosphere suggest that a methane-bearing atmosphere could have existed up to ~50 km altitude (Fig. 4)[29], and this could represent the hypothesised transition between poorly mixing upper and lower atmospheric domains. However, micrometeorites cannot test the altitude of this transition since they are quench crystallised by the time they reach ~75 km. The only work similar to that presented here is an analysis of the oxidation state of impact ejecta preserved in 3.24 billion year old spherule beds, which found significant heterogeneity in oxidation state and that atmospheric oxygen fugacity was $<10^{-4}$ bar at this time[30]. Although Krull-Davatzes et al.[30] suggested that the oxidation state of impact ejecta is set within the ejection plume (see also references therein), and thus impact spherules represent samples of the lower atmosphere, it is plausible that some are remelted during reentry[31]. Because impact spherules are significantly larger than micrometeorites and reenter the atmosphere at lower velocity, those that remelted would sample a thicker belt and lower level of the atmosphere, possibly close to the hypothesised oxygen transition. Detailed modelling of impact spherule reentry thus represents a possible avenue for sampling the chemistry of middle levels of the atmosphere; in particular, larger particles are more likely to have been remelted, so certain size fractions may have sampled appropriate atmospheric levels.

Chemical models of the Archaean atmosphere are based on gas fluxes from modern volcanoes and the effects of UV photolysis on those gases, and constrained by the above

observations from ancient rocks[23]. These models imply that at lower atmospheric levels, reaction with abundant volcano-derived H_2 gas eliminated free O_2, consistent with the $\Delta^{33}S$ data that require an oxygen-poor lower atmosphere. Above ~50 km photolysis of CO_2 produced O_2 and CO (Fig. 4; Ref. 29), but there is extensive debate about how much CO_2 was present in the Archaean atmosphere[23], with estimates ranging from 10 – 1000 PAL. The more CO_2 present in these models, the more O_2 and CO is produced by photolysis in the upper atmosphere. Furthermore, these models suggest that there may have been more CO produced than O_2; for example, the model in Figure 4 suggests an upper atmosphere with O_2/CO of ~0.2. However, this abundant CO is inconsistent with the observed magnetite-rich micrometeorites because it would act as a reductant (e.g., CO + FeO = CO_2 + Fe; Extended Data Fig. 5). At equilibrium, the point where oxidation balances reduction comes when there is half as much O_2 as CO, so any oxidation implies O_2/CO > 0.5. If the O_2/CO ratio was only slightly greater than 0.5, the oxidation would have been sluggish and we would only see thin wüstite rims on metal in the larger spherules. Given that most of these very small micrometeorites were completely oxidised to magnetite, the Archaean upper atmosphere must have been characterised by elevated O_2 approaching modern abundances, requiring relatively abundant CO_2 as a source of O_2, and elevated O_2/CO.

References

1 Lyons, T. W., Reinhard, C. T. & Planavsky, N. J. The rise of oxygen in Earth's early ocean and atmosphere. *Nature* **506**, 307-315 (2014).

2 Farquhar, J., Zerkle, A. L. & Bekker, A. in *Treatise in Geochemistry* Vol. 6: The Atmosphere - History (eds H. Holland & K. Turekian) 91-138 (2014).

3 Som, S. M., Catling, D. C., Harnmeijer, J. P., Polivka, P. M. & Buick, R. Air density 2.7 billion years ago limited to less than twice modern levels by fossil raindrop imprints. *Nature* **484**, 359–362 (2012).
4 Pavlov, A. A. & Kasting, J. F. Mass-independent fractionation of sulfur isotopes in Archean sediments: Strong evidence for an anoxic Archean atmosphere. *Astrobiology* **2**, 27–41 (2002).
5 Rasmussen, B. & Buick, R. Redox state of the Archean atmosphere: Evidence from detrital heavy minerals in ca. 3250–2750 Ma sandstones from the Pilbara Craton, Australia. *Geology* **27**, 115–118 (1999).
6 Rye, R. & Holland, H. D. Paleosols and the evolution of atmospheric oxygen: A critical review. *American Journal of Science* **298**, 621–672 (1998).
7 Bekker, A. *et al.* Iron formation: The sedimentary product of a complex interplay among mantle, tectonic, and biospheric processes. *Economic Geology* **105**, 467-508 (2010).
8 Buick, R. The antiquity of oxygenic photosynthesis: Evidence from stromatolites in sulphate-deficient Archaean lakes. *Science* **255**, 74-77 (1992).
9 Eigenbrode, J. L. & Freeman, K. H. Late Archean rise of aerobic microbial ecosystems. *Proceedings of the National Academy of Sciences* **103**, 15759–15764 (2006).
10 Konhauser, K. O. *et al.* Oceanic nickel depletion and a methanogen famine before the Great Oxidation Event. *Nature* **458**, 750-753 (2009).
11 Farquhar, J. & Wing, B. A. Multiple sulfur isotopes and the evolution of the atmosphere. *Earth and Planetary Science Letters* **213**, 1–13 (2003).
12 Cioni, R., Marianelli, P., Santacroce, R. & Sbrana, A. in *Encyclopedia of Volcanoes* (ed H. Sigurdsson) 477 - 494 (Academic Press, 2000).
13 Finlayson-Pitts, B. & Pitts, J. *Chemistry of the upper and lower atmosphere: Theory, experiments, and applications*. (Elsevier, 1999).
14 Love, S. G. & Brownlee, D. E. Heating and thermal transformation of micrometeoroids entering the Earth's atmosphere. *Icarus* **89**, 26-43 (1991).
15 Rietmeijer, F. J. M. & Nuth, J. A. Collected extraterrestrial materials: Constraints on meteor and fireball compositions. *Earth, Moon Planets* **82-83**, 325-350 (2000).
16 Genge, M., Engrand, C., Gounelle, M. & Taylor, S. The classification of micrometeorites. *Meteoritics and Planetary Science* **43**, 497-515 (2008).
17 Tianrui, S., Zhengjun, H., Yusheng, W. & Yanxue, L. A study of Mesoproterozoic iron cosmic micro-spherules from 1.8 Ga and 1.6 Ga old strata in the Ming Tombs District, Beijing. *Acta Geologica Sinica* **81**, 649-657 (2007).
18 Awramik, S. M. & Bucheim, H. P. A giant, Late Archean lake system: The Meentheena Member (Tumbiana Formation; Fortescue Group), Western Australia. *Precambrian Research* **174**, 215-240 (2009).
19 Blake, T. S., Buick, R., Brown, S. J. A. & Barley, M. E. Geochronology of a Late Archaean flood basalt province in the Pilbara Craton, Australia: Constraints on basin evolution, volcanic and sedimentary accumulation, and continental drift rates. *Precambrian Research* **133**, 143-173 (2004).
20 Trendall, A. F., Compston, W., Nelson, D. R., De Laeter, J. R. & Bennett, V. C. SHRIMP zircon ages constraining the depositional chronology of the Hamersley Group, Western Australia. *Australian Journal of Earth Sciences* **51**, 621-644 (2004).
21 Rudraswami, N. G. *et al.* Refractory metal nuggets in different types of cosmic spherules. *Geochimica et Cosmochimica Acta* **131**, 247-266 (2014).

22 Chevrier, V., Rochette, P., Mathe, P.-E. & Grauby, O. Weathering of iron-rich phases in simulated Martian atmospheres. *Geology* **32**, 1033-1036 (2004).
23 Kasting, J. F. in *Treatise in Geochemistry* Vol. 6: The Atmosphere - History (eds H. Holland & K. Turekian) 157-175 (2014).
24 Abuluwefa, H. T., Guthrie, R. I. L. & Ajersch, F. Oxidation of low carbon steel in multicomponent gases: Part I. Reaction mechanisms during isothermal oxidation. *Metallurgical and Materials Transactions A* **28A**, 1633-1641 (1997).
25 Bredesen, R. & Kofstad, P. On the oxidation of iron in CO_2 + CO mixtures. III: Coupled linear parabolic kinetics. *Oxidation of Metals* **36**, 27-56 (1991).
26 Genge, M. The origins of I-type spherules and the atmospheric entry of iron micrometeoroids. Meteoritics and Planetary Sciences (In Press).
27 Legras, B., Joseph, B. & Lefevre, F. Vertical diffusivity in the lower stratosphere from Lagrangian back-trajectory reconstructions of ozone profiles. *Journal of Geophysical Research* **108** (2003).
28 Fulchignoni, M. *et al.* In situ measurements of the physical characteristics of Titan's environment. *Nature* **438**, 785-791 (2005).
29 Zahnle, K., Claire, M. & Catling, D. The loss of mass-independent fractionation in sulfur due to a Palaeoproterozoic collapse of atmospheric methane. *Geobiology* **4**, 271-283 (2006).
30 Krull-Davatzes, A. E., Byerley, G. R. & Lowe, D. R. Evidence for a low-O_2 Archean atmosphere from nickel-rich chrome spinels in 3.24 Ga impact spherules, Barberton greenstone belt, South Africa. *Earth and Planetary Science Letters* **296**, 319-328 (2010).
31 Goldin, T. J. & Melosh, H. J. Self-shielding of thermal radiation by Chicxulub impact ejecta: Firestorm or fizzle? *Geology* **37**, 1135–1138 (2009).

Author Contributions

A.G.T. conceptualised the project, conducted fieldwork and EMP analysis, and wrote the paper. L.B. conducted fieldwork, micrometeorite separation and SEM analysis. M.G. generated the micrometeorite oxidation model. S.A.W. advised on micrometeorite separation, conducted Raman spectroscopy and interpreted synchrotron results. H.E.A.B. conducted the synchrotron analysis. J.L.W. modelled the oxidising conditions imposed at equilibrium by different atmospheres. All authors reviewed the paper prior to submission.

Acknowledgements

We thank N. Wilson and A. Langendam for assistance with electron microprobe work and electron microscopy respectively. The authors acknowledge use of the Monash

Centre for Electron Microscopy, and CSIRO Microbeam Lab. Part of this research was undertaken on the Powder diffraction beamline at the Australian Synchrotron, Victoria, Australia. M.G. acknowledges STFC grant number ST/J001260/1. Five anonymous reviewers are thanked for their constructive reviews, and the Senior Editor for editorial handling, which significantly improved the manuscript.

Author Information

The authors declare no competing financial interests. Correspondence and requests for materials should be addressed to A.G.T. (andrew.tomkins@monash.edu).

Figures

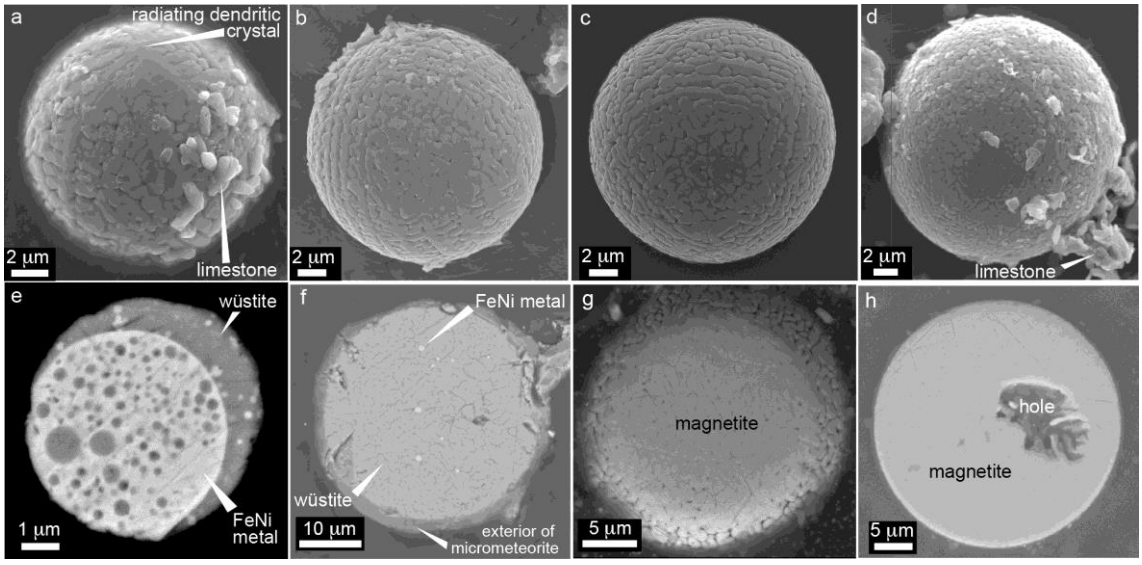

Figure 1 Examples of fossil micrometeorites recovered in this study. The top panels show representative examples of surface features of the micrometeorites, characterised by interlocking dendritic iron oxide crystals. The lower panels show representative examples of their internal features. The majority of micrometeorites that we sectioned

were identical to the magnetite-only examples shown on the right. The metal-dominated sample is the only one we observed; the spheres of wüstite in metal indicate mingling of immiscible melts. The small size of this example is consistent with the enhanced preservation of metal in smaller micrometeorites predicted by the oxidation modeling (Fig. 2).

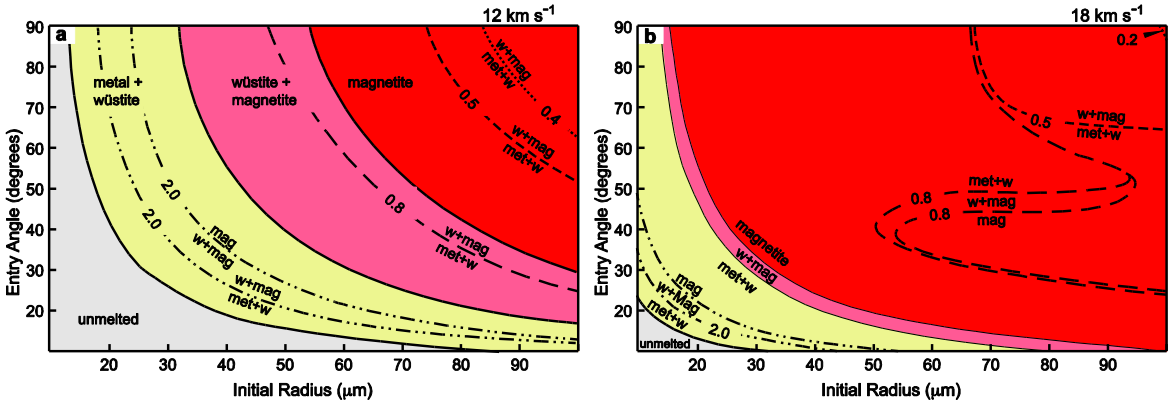

338

339

340 **Figure 2** Results of the atmospheric oxidation model, showing the stability fields
341 for the dominant iron-bearing phases after heating (Met – metal, W – wüstite, Mag –
342 magnetite) relative to the size and entry angle of particles. Results are given for two
343 different entry velocities: 12 km s^{-1} is the minimum possible entry velocity, and 18 km s^{-1}
344 is a common velocity for meteoroids that survive atmospheric entry. The coloured
345 stability fields are for the current atmospheric oxygen abundance, dashed lines indicate
346 the shift in these fields at different oxygen abundances (0.2, 0.5, 0.8, and 2.0 x PAL).

347

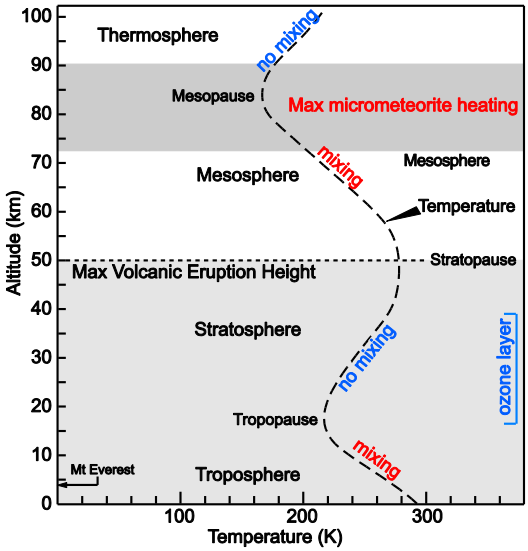

Figure 3 Profile of the modern atmosphere showing the altitudes reached by volcanic eruptions compared with that of maximum micrometeorite heating, as well as the temperature profile and how this influences vertical mixing.

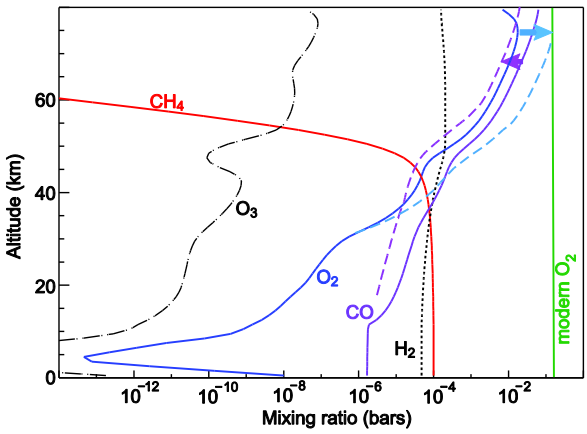

Figure 4 A recent model of the Archaean atmosphere that includes methane, showing the effects of CO_2 photolysis on O_2 and CO concentration (modified from ref. 29 with permission from John Wiley and Sons, license number 3816161033966). The solid blue and purple lines indicate the estimated O_2 and CO concentrations of the existing

model[29], whereas the dashed blue and purple lines approximate the relatively small shifts in the positions of these lines needed to satisfy the observed micrometeorite oxidation.

Methods

The weathered exterior of the limestone blocks was removed using a diamond saw. The resulting samples (3.6 kg) were then crushed to <1 cm fragments, then bathed in 10% HCl (samples 1.1, 1.3a) or 20% HCl (sample 1.2) for 1-2 days. After wet sieving the residues into 20-125, 125-355, 355-1000 and >1000 μm size fractions, magnetic separation and hand picking under a binocular microscope were used to isolate micrometeorites. Care was taken at all stages to keep the samples covered, to avoid contamination by present day micrometeorites. The isolated grains were then confirmed or rejected as micrometeorites through imaging using a JEOL 7001F FEG-SEM. Micrometeorites were then embedded in epoxy and sectioned for further imaging and electron microprobe (EMP) analysis using a JEOL 8500F HyperProbe operating at 15 kV accelerating voltage and 20 nA beam current. Eleven micrometeorites were sectioned effectively due to their small size.

Raman spectroscopy was used to confirm the EMP-determined identity of wüstite in Figure 1F. Raman spectra were collected using a Renishaw 'Invia' Raman Microscope fitted with a coherent 632.8 nm HeNe laser. The 520.5 cm^{-1} band of a silicon wafer was used to calibrate the instrument prior to analysis of samples. Spectra were recorded between 2000 and 100 cm^{-1} with a resolution of 1–2 cm^{-1} using a 50x objective lens. An initial spectrum was recorded using a power of ~1.5 mW at the sample surface and an exposure time of 60 s for 4 accumulations. The resulting spectrum (Extended Data Fig. 3A) is characterised by a broad, asymmetrical band at 650–660 cm^{-1}, which is consistent with the spectrum of wüstite[32] (Extended Data Fig. 3B). Although magnetite also produces a band in the vicinity of 660–680 cm^{-1}, the diagnostic peaks of magnetite at ~300 and ~535 cm^{-1} are not observed in this spectrum. A second test of the wüstite identification is possible because wüstite decomposes rapidly to hematite when exposed to 632.8 nm radiation at ~7.0 mW, whereas magnetite is stable at these conditions[32]. Thus a second spectrum was recorded using ~7.5 mW at the sample surface, and a single accumulation with an exposure time of 50 s. In this acquisition, the targeted iron oxide phase immediately decomposed to produce the characteristic spectrum of hematite (Extended Data Fig. 3A), confirming the identity of wüstite.

An additional six whole micrometeorites were mounted on Hampton Scientific CryoLoops to investigate whether multiple phases could be identified within whole micrometeorite samples via Powder X-ray diffraction (XRD). Data were collected on these using the Powder Diffraction beamline at the Australian Synchrotron. The penetration depth of the X-ray beam employed (15.0 keV) is on the order of 50 μm in magnetite, which allows for non-destructive sampling of the entire volume of individual micrometeorites. Data were collected with the MYTHEN-II strip detector. Mineral phases were identified with reference to the ICDD PDF-2 database using the EVA V.1 software package available from Bruker AXS. Due to their small size, reliable XRD data could only be obtained for two micrometeorites; results are shown in Extended Data Fig. 4).

To evaluate the oxidising potential of different atmospheres, equilibrium gas speciation (and hence fO_2) was determined by gibbs free energy minimsation calculations using the HSC Chemistry (v. 6.1) software package. Modelling was undertaken between

1250 and 2500°C, and 1 to 1×10^{-6} bar pressure, assuming ideal gas mixing. For the CO_2-CO and CO_2 gas mixtures species were limited to O_2, CO and CO_2, and N_2 is considered to have no oxidising or reducing capacity. For air species included in the modelling were CO, CO_2, H, H_2, HNO, HNO_2, HNO_3, HO_2, H_2O, N, N_2, NO, NO_2, NO_3, N_2O, O, O_2, O_3, OH, Ar. Results for the range of dynamic ram pressures experienced by micrometeorites are shown in Extended Data Figure 5.

The model used to calculate the extent of oxidation of iron metal during atmospheric entry is based on the model of Ref. 14 and numerically integrates the partial differential equations for motion, heat and mass of particles decelerating in the atmosphere. Evaporation of particles is modelled using the Langmuir equation with coefficients for iron metal and iron oxide melts derived from experimental studies[33]. Evaporative mass loss is used in the model to calculate the change in mass and radius of the particle, which directly influences its deceleration. The average density of the particles is assumed to be that of wüstite, given that most of the observed particles are dominated by iron oxides and that the density of wüstite is between that of magnetite and iron. The latent heat of evaporation is considered in evaluating the temperature of the particle, together with heat loss by thermal radiation and energy input due to incident atmospheric molecules. As in Love and Brownlee[14], the trajectory of the particle, derived from the equations of motion, is used to trace change in altitude at each time step and thus atmospheric density. Time steps of 0.01 seconds were used for these simulations; results are independent of time step size to within 1% for the peak temperature of particles. The degree of oxidation is calculated from the mass of oxygen that particles encounter during deceleration, moderated by loss of oxygen by evaporation of iron oxide liquid. This calculation recognises that the amount of oxygen accreted by iron micrometeorites can be no more than the mass of oxygen the particles encounter during deceleration. It also uses the observation that iron oxide liquid mantles the iron metal core of the particle due to surface tension effects resulting in evaporation of oxide rather than metal. Accretion of oxygen is also assumed to only occur when particles are molten since diffusion rates within solid metal are too slow to allow significant oxidation over the few seconds of deceleration.

Given the dependence of the extent of oxidation on both particle temperature and mass of oxygen encountered, the atmospheric density-altitude profile is important. In the absence of a consensus density model of the Archaean atmosphere the 1976 U.S. Standard Atmosphere is used in the simulations. Some models of the Archaean atmosphere, however, suggest that density variation with altitude was similar to the modern day[3]. Changes in the exact atmospheric density with altitude, however, can be seen to change the mass of gas encountered over molten flight relatively little. A denser Archaean atmosphere results in a larger mass of gas encountered per second, but particle deceleration would also occur more rapidly, giving a shorter period for accretion of oxygen. Conversely a less dense Archaean atmosphere results in a smaller mass of gas encountered per second but less deceleration resulting in a longer period over which particles accrete oxygen. The results of 12,000 simulations with and without oxidation suggest that iron micrometeoroids undergo maximum heating at altitudes equivalent to 65-90 km; i.e., within the current day mesosphere.

The abundance of oxygen in the Archaean atmosphere in the simulations was varied by scaling the modern day oxygen abundance with altitude. The effects of other gas species on oxidation or reduction were not considered within the model. Carbon monoxide, if present within the Archaean atmosphere, would oppose oxidation by driving reduction of iron oxide melt and production of CO_2. At equilibrium, if the O_2/CO ratio was < 0.5, the metal would not be oxidised (i.e., $2Fe + O_2 = 2FeO$ versus $FeO + CO = Fe$

458 + CO_2). The abundances of oxygen used within the model can therefore be considered to
459 be those in excess of reducing species in the atmosphere, although in disequilibrium
460 scenario of micrometeorite entry the rate of oxidation by O_2 may be faster than the rate
461 of reduction by CO. The important criteria within the oxidation model are, the abundance
462 of oxygen compared to present atmosphere, the atmospheric density profile and the
463 molten flight time of the particle, and the entry parameters that determine peak
464 temperature and altitude of peak temperature. The objective of the simulations is not to
465 provide an accurate and realistic model of Archaean atmospheric chemistry, but simply
466 to estimate the abundance of free oxygen available to produce net oxidation, required to
467 explain the presence of magnetite-rich Archaean I-type spherules. Even if the mass of
468 oxygen accreted by particles predicted by the simulations is subject to an error of an order
469 of magnitude, the results would still necessitate abundant oxygen within the Archaean
470 upper atmosphere, of a significant fraction of the modern day.
471

472 **Methods References**

473

474 32 de Faria, D. L. A., Silva, S. V. & De Oliveira, M. T. Raman microspectroscopy
475 of some iron oxides and oxyhydroxides. *Journal of Raman Spectroscopy* **28**,
476 873-878 (1997).
477 33 Wang, J., Davis, A. M., Clayton, R. N. & Mayeda, T. K. in *25th Lunar and*
478 *Planetary Science Conference.* 1459–1460. (1994).

479

480

481 **Extended Data**

Sample ID	1.1(2)	1.1(2)	1.1(2)	1.1(2)	1.1(2)	1.3(a)*
Fe (at.%)	43.46	43.82	42.74	50.07	50.35	90.16
Ni (at.%)	0.00	0.00	0.00	0.00	0.00	6.41
O (at.%)	56.54	56.18	57.26	49.93	49.65	3.43
Formula	Fe_3O_4	Fe_3O_4	Fe_3O_4	FeO	FeO	FeNi + FeO
Mineral	magnetite	magnetite	magnetite	wüstite	wüstite	metal + wüstite†

*This analysis comes from the metal particle rimmed by wüstite in Fig. 1e.
†Owing to the small size of the metal particles, analyses of these invariably included some surrounding wüstite in the total.

482

483 **Extended Data Table 1.** Representative analyses of magnetite, wüstite and metal.

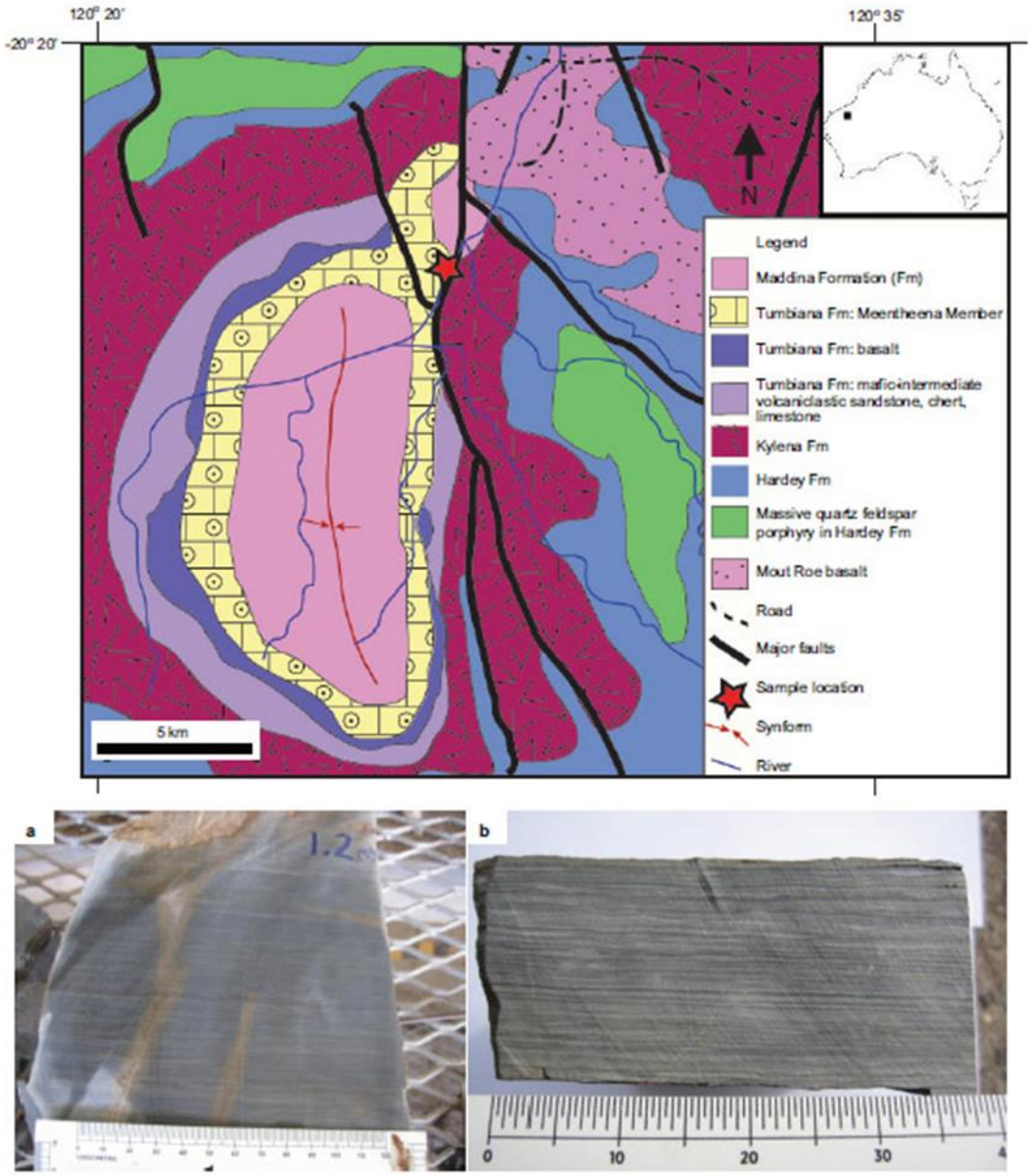

Extended Data Figure 1 Geological map showing the context of the sampling location (red star), and examples of the samples used in the study. The samples in photos A and B show examples of the fine laminations that occur in some layers of this unit. In A, buff coloured zones along cracks highlight examples of modern day oxidative weathering, whereas the grey colouration of the remainder of the sample indicates that it was not weathered, allowing survival of the micrometeorites. Weathered rock was removed using a diamond saw prior to micrometeorite separation.

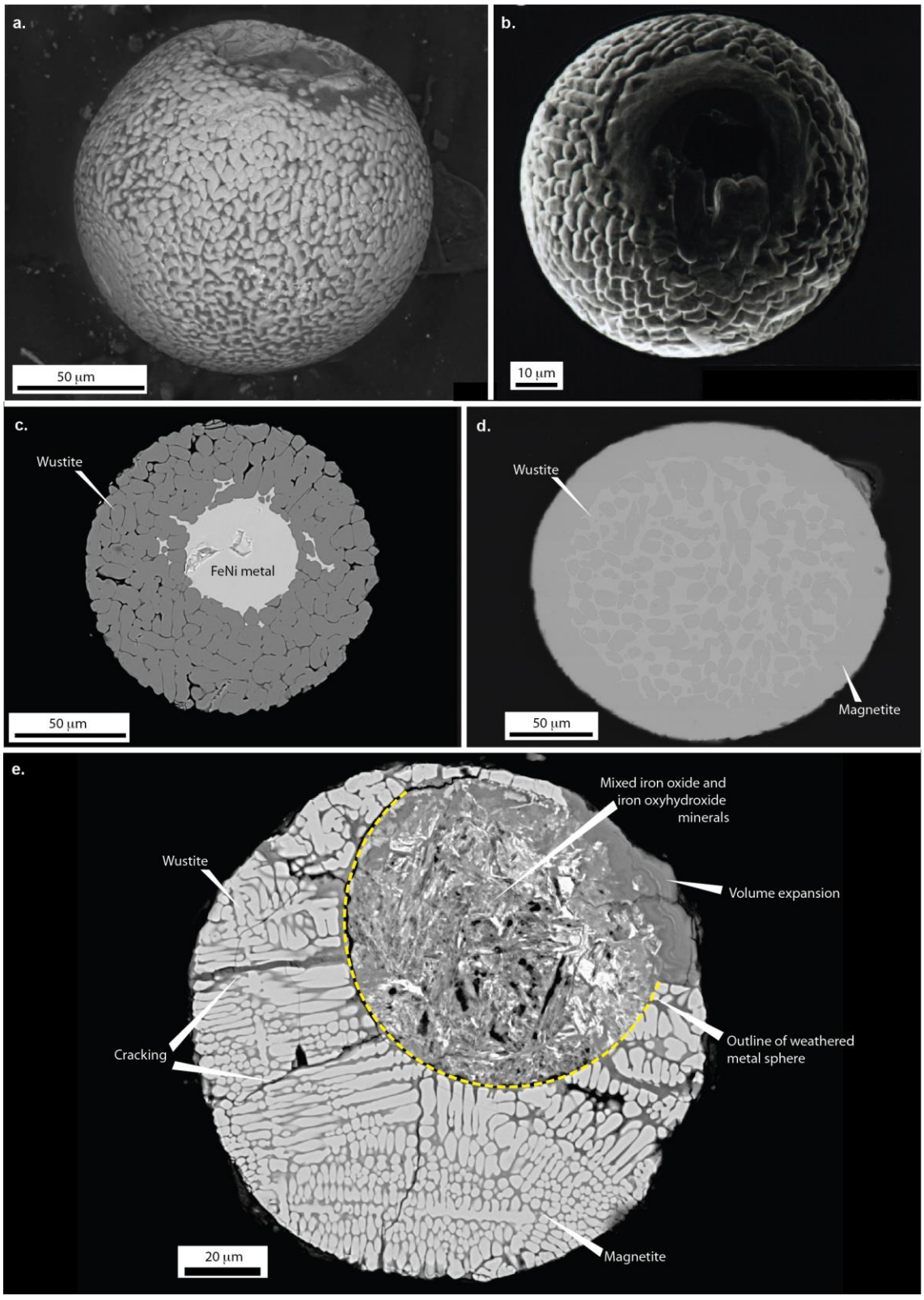

Extended Data Figure 2 Examples of modern iron-type micrometeorites collected from the Antarctic ice sheet. The top panels are secondary electron images showing the exterior morphology. The center panels show back-scattered electron (BSE) images

highlighting the interior mineralogical variation. In (e) is a BSE image showing an example of a partially weathered modern micrometeorite where the metal has been replaced by iron oxides and iron oxyhydroxides after arriving on the surface; expansion has led to cracking in the surrounding wüstite and magnetite, which would destroy the micrometeorite if continued. Note that the wüstite and magnetite are unaffected by the weathering. All imaging by M. Genge.

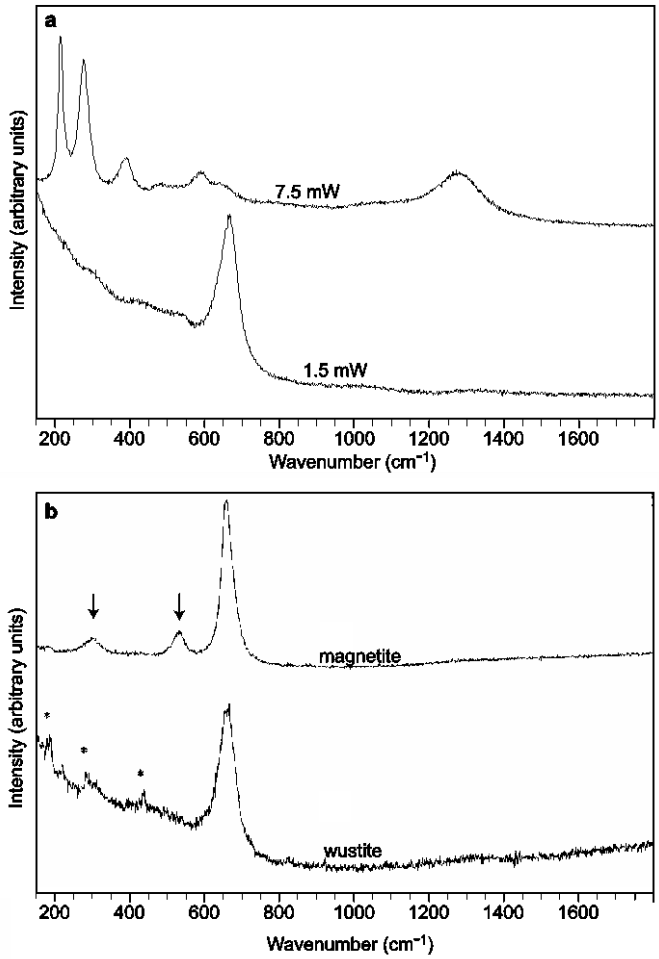

Extended Data Figure 3 Results of laser Raman spectroscopy confirming the identity of wüstite. Wüstite is metastable below 570°C and decomposes to hematite when higher laser power is used, whereas magnetite does not decompose in this fashion[32]. The iron oxide in the sectioned micrometeorite shown in Figure 1F gave the spectra shown in Panel A at 1.5 mW and decomposed to produce spectra B at 7.5 mW laser power,

consistent with the characteristics of wüstite. Panel B shows the characteristic spectra of magnetite and wüstite from Ref. 32; note the arrowed bumps that characterize magnetite, which are missing in wüstite, and the broadened main peak of wüstite.

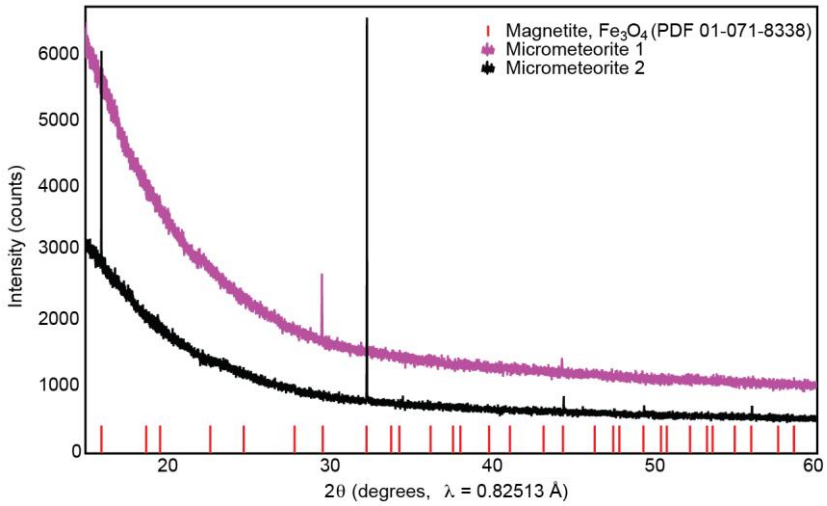

Extended Data Figure 4 Two synchrotron powder X-ray diffraction patterns, each collected from a single micrometeorite. Not all major Bragg peaks for magnetite are detected, and deviation from the expected relative intensities of peaks is observed, as a consequence of poor particle size statistics.

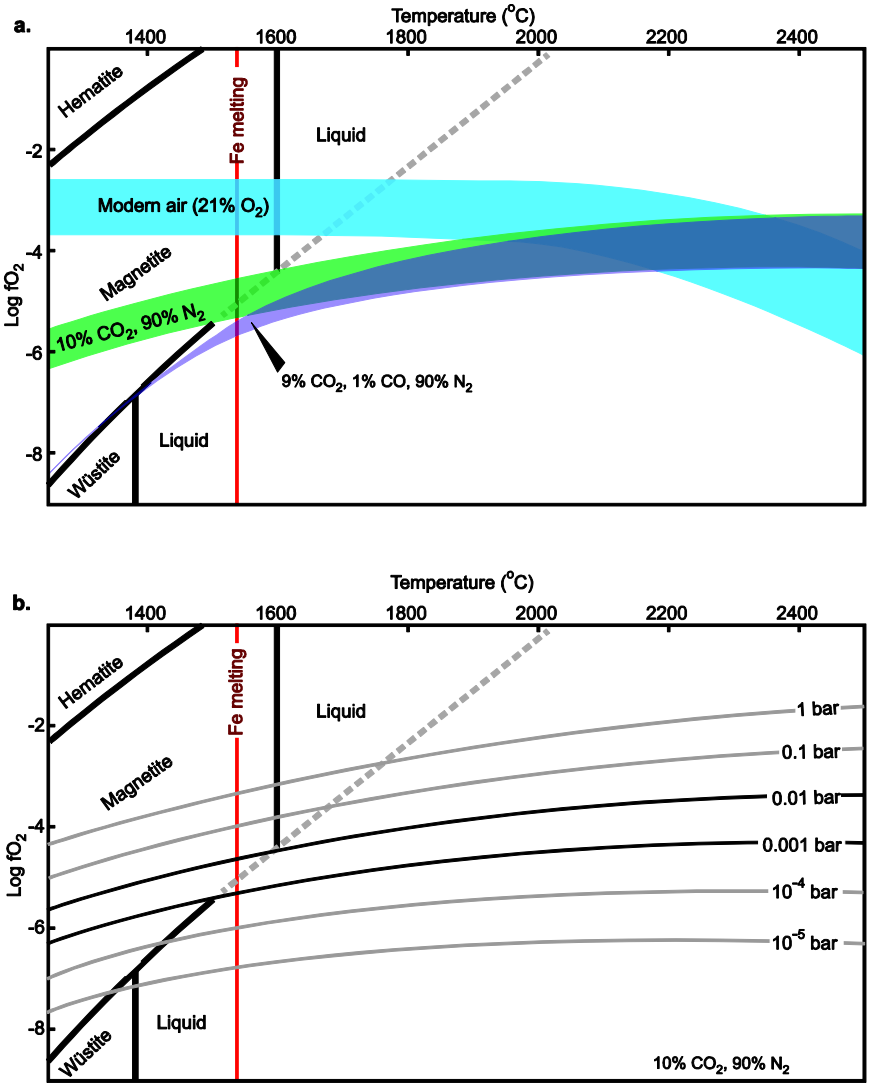

Extended Data Figure 5 Equilibrium modelling of the oxidising conditions imposed by different atmospheres relative to the stability fields of hematite, magnetite and wüstite. These models represent the stability fields at equilibrium and do not consider the time needed to attain equilibrium (refer to Ext. Data Fig. 6). In (a) the top of each coloured band represents the conditions imposed by the maximum dynamic ram pressure (0.02 bar) experienced by micrometeorites, which applies to the largest and fastest micrometeorites; the bottom of each band is more relevant to the small micrometeorites observed in this study (0.001 bar). In (b) the model for an atmosphere containing 90% N_2 and 10% CO_2 is shown with contours for pressure to allow a comparison with atmospheres of different CO_2 abundance.

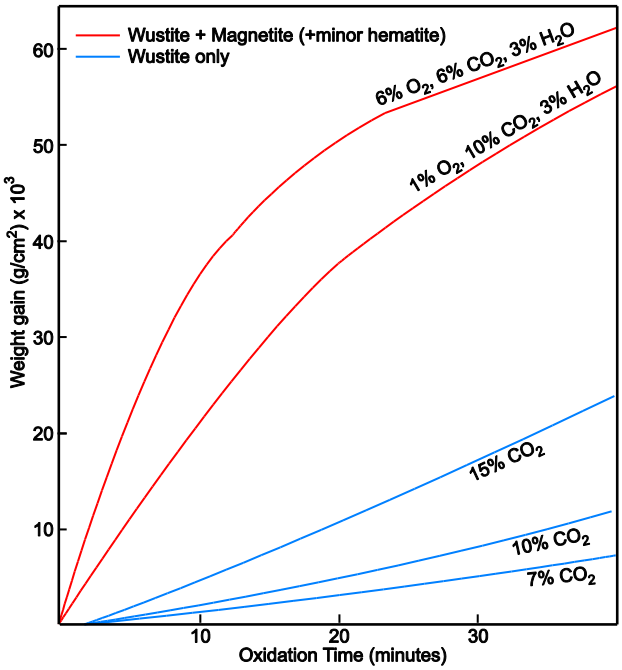

527

528 **Extended Data Figure 6** Results of experiments on oxidation of low carbon
529 steel in different gas mixes; compiled by amalgamating Figures 1 and 8 in Ref. 24. These
530 are the results of experiments conducted at 1100°C and atmospheric pressure (1 bar), the
531 remaining gas being N_2; oxidation was measured by progressive weight gain over time.
532 The conditions of survivable micrometeorite entry are: 400 – 2800°C and dynamic ram
533 pressure on the order of 0.001 – 0.02 bar for < 2 seconds. Higher temperatures result in
534 more effective oxidation, lower pressures result in less effective oxidation.

535

536 a.

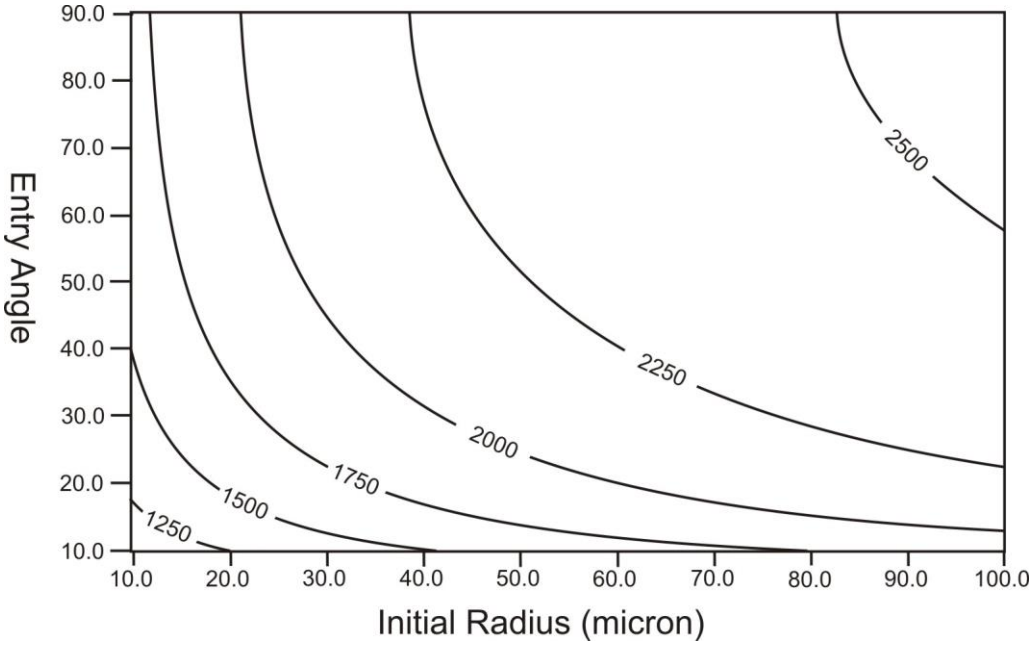

537

538 b.

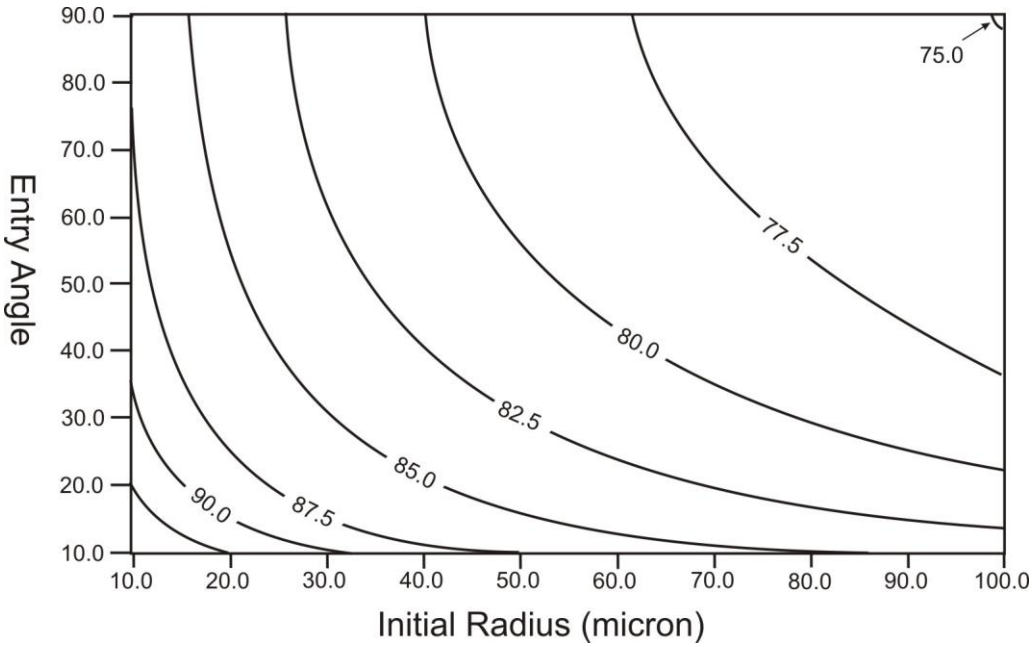

539

540

c.

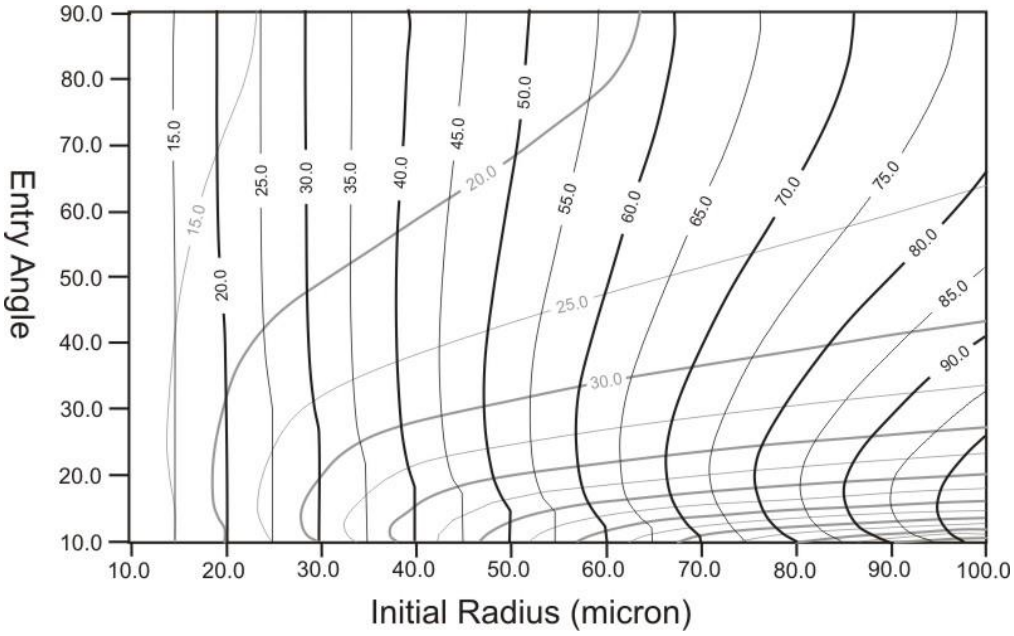

Extended Data Figure 7 Results of atmospheric entry modeling. (a) The peak temperatures reached by I-type spherules entering the atmosphere at 12 km s^{-1}. Note that heating is greater for larger particles undergoing vertical atmospheric entry. The high density of metal micrometeoroids leads to higher peak temperatures than silicate-dominated particles. (b) The altitude at which peak temperature is reached for I-type spherules with an entry velocity of 12 km s^{-1}. Particles with higher entry velocity have similar peak altitudes since mass loss through evaporation leads to increased deceleration. (c) The final radii of I-type particles after deceleration at entry velocities of 12 km s^{-1} (black) and 18 km s^{-1} (grey). Significant mass loss occurs at higher entry velocities, entry angles and particle sizes. Mass loss occurs by surface evaporation of the exterior oxide melt.